Attenuated response to liver injury in moesin-deficient mice: Impaired stellate cell migration and decreased fibrosis

Tokunari Okayama [a,1], Shojiro Kikuchi [a,*,1], Toshiya Ochiai [a], Hisashi Ikoma [a], Takeshi Kubota [a], Daisuke Ichikawa [a], Hitoshi Fujiwara [a], Kazuma Okamoto [a], Chouhei Sakakura [a], Teruhisa Sonoyama [a], Yukihito Kokuba [a], Yoshinori Doi [b], Sachiko Tsukita [c], D. Montgomery Bissell [d], Eigo Otsuji [a]

[a] Department of Surgery, Kyoto Prefectural University of Medicine, Kamigyo-ku, Kyoto 602-8566, Japan
[b] Department of Internal Medicine, Otemae Hospital, Chuo-ku, Osaka 540-0008, Japan
[c] Laboratory of Biological Science, Organismal Biosystems Laboratory, Graduate School of Frontier Biosciences/Department of Pathology, Graduate School of Medicine, Osaka University, Osaka 565-0871, Japan
[d] Department of Medicine and Liver Center, University of California, San Francisco, California 94143, USA

ARTICLE INFO

ABSTRACT

Hepatic stellate cells (HSCs) respond to injury with a coordinated set of events (termed activation), which includes migration and upregulation of matrix protein production. Cell migration requires an intact actin cytoskeleton that is linked to the plasma membrane by ezrin–radixin–moesin (ERM) proteins. We have previously found that the linker protein in HSCs is exclusively moesin. Here, we describe HSC migration and fibrogenesis in moesin-deficient mice. We developed an acute liver injury model that involved focal thermal denaturation and common bile duct ligation. HSC migration and collagen deposition were assessed by immunohistology and quantitative real-time PCR. Activated HSCs were isolated from wild-type or moesin-deficient mice for direct examination of migration. Activated HSCs from wild-type mice were positive for moesin. Migration of moesin-deficient HSCs was significantly reduced. In a culture assay, 22.1% of normal HSCs migrated across a filter in 36h. In contrast, only 1.3% of activated moesin-deficient HSCs migrated. Collagen deposition around the injury area similarly was reduced in moesin-deficient liver. The linker protein moesin is essential for HSC activation and migration in response to injury. Fibrogenesis is coupled to migration and reduced in moesin-deficient mice. Agents that target moesin may be beneficial for chronic progressive fibrosis.

© 2008 Elsevier B.V. All rights reserved.

1. Introduction

The response to liver injury is multi-faceted, involving several cell types and elaboration of a collagen-rich extracellular neomatrix, which serves both to strengthen the tissue and as a scaffolding upon which repair events proceed. Over time, the neomatrix undergoes chemical changes that render it resistant to degradation. Hence, the interest in strategies to modulate fibrogenesis. Hepatic stellate cells (HSCs) are prominent in the repair response as the principal source of extracellular matrix. They are also motile and migrate to the injury site. Migration appears to be among the initial responses to injury. The chemoattractant for HSC migration and intracellular signaling pathways has been defined [1]. The cells appear to utilize a pathway that consists of hyaluronic acid and CD44, a cognate receptor for this matrix constituent [2]. Migration also requires mechanical force generation, which is mediated by the actin cytoskeleton. The latter structure comprises actin linked to the plasma membrane by a protein of the ezrin–radixin–moesin (ERM) family, which forms a complex with a variety of other membrane-associated proteins [3–6].

The ERM components in HSCs have not been defined, nor have their role in cell migration after acute injury. Many fibroblastic cells contain more than one ERM protein. We showed that HSCs, in contrast, contain only moesin. We studied migration and activation of HSCs with or without moesin, after an injury challenge. HSCs from mice lacking moesin displayed significantly impaired migration and activation relative to those in wild-type cells. Fibrogenesis was decreased in parallel.

2. Materials and methods

2.1. Animals

We have previously generated moesin-deficient ($Msn^{-/-}$) mice on a mixed genetic background (129/Sv × C57BL/6J) [7]. The mice were back-crossed through more than eight generations to create congenic C57BL/6J $Msn^{-/-}$ mice. All experiments were carried out in accordance with guidelines established by the Guidelines for Animal Experiments of Kyoto Prefectural University of Medicine, Kyoto, Japan.

2.2. Antibodies and reagents

Rabbit polyclonal antibodies (TK89, anti-mouse ERM) and monoclonal antibodies (M11, anti-mouse ezrin; R21, anti-mouse radixin; M22, anti-mouse moesin) were provided by the Department of Cell Biology, Faculty of Medicine, Kyoto University, Japan [8]. Anti-α-smooth muscle actin (SMA)/FITC-conjugated monoclonal antibody was purchased from Sigma–Aldrich (St. Louis, MO, USA). Alexa Fluor 546-conjugated secondary antibody was used (Invitrogen, Molecular Probes). Sevoflurane (Sevofrane®) for anesthesia was from Abbott (Chicago, IL, USA). Collagen was visualized with 0.1% Sirius Red solution (Polysciences, Warrington, PA, USA) saturated in picric acid solution (Wako, Tokyo, Japan). Collagenase was from Nacalai Tesque (Tokyo, Japan), pronase and DNase from Roche (Basel, Switzerland), and Opti prep® from Axis-Shield PoCAS (Oslo, Norway). Ham's Nutrient Mixture F12 and Dulbecco's Modified Eagle's Medium (DMEM) were from Nissui Pharmaceutical (Tokyo, Japan) and ASF104 culture medium from Ajinomoto (Tokyo, Japan). Cell culture inserts were pre-coated with hyaluronic acid (sodium salt, 1mg/ml) from *Streptococcus equi* (BioChemica, Melbourne, FL, USA) before the migration assay.

2.3. Surgical procedures

2.3.1. Biliary obstruction model by common bile duct ligation

For studies of liver fibrosis and HSC activation *in vivo*, the common bile duct was ligated. Seven days later, the mice were sacrificed to isolate HSCs for liver perfusion, as described previously [2]. For histological examination, the mice were sacrificed on 7 and 14 days after operation.

2.3.2. Hepatic injury model by thermal denaturation

The injury device was an electrically heated probe with a beveled tip of 2mm diameter, which was set at 150 °C (Taiyo Electric, Hiroshima, Japan). A 1-s application of the tip to the surface of the liver reproducibly resulted in a hemispheric injury of 3 mm diameter. Two lesions were created in the left lobe and one in the right lobe. Mice were sacrificed after 1 or 2 weeks, with removal of the whole liver, including the adherent peritoneal wall (including parietal peritoneum and muscle). The reason for this procedure was to remove completely and keep the fragile injured liver surface. Each experimental group consisted of 4–6 mice.

2.4. Histology and immunofluorescent microscopy

For *in situ* histology, the liver was perfused sequentially with PBS (pH 7.4) and 4% phosphate-buffered formaldehyde. Tissue sections (5µm) were treated with xylene, and rehydrated with decreasing graded ethanol. Hematoxylin stain and Sirius Red stain were performed for histological analysis and collagen visualization, respectively. For immunofluorescent staining of normal or bile duct ligation (BDL) mouse livers, the liver was removed from $Msn^{+/+}$ and $Msn^{-/-}$ mice, cut into small pieces, and frozen in liquid nitrogen. Frozen sections were cut on a cryostat, mounted onto cover glasses, air dried, and fixed with 95% ethanol for 15 min at 4 °C, followed by 100% acetone for 1min at room temperature. A pair of frozen sections from the $Msn^{+/+}$ and $Msn^{-/-}$ liver was placed on the same cover glass and processed for double staining with the appropriate antibodies. The images were obtained with a fluorescence microscopy (model IX71; Olympus, Tokyo, Japan) and DP Manager (Olympus). *In vivo*-activated HSCs were cultured for 2days, and then treated with rat anti-ERM monoclonal antibody (M11, anti-mouse ezrin; R21, anti-mouse radixin; M22, anti-mouse moesin). Secondary antibodies were conjugates of Alexa Fluor 546 (Molecular Probes). FITC-conjugated anti-α-SMA was used for double staining.
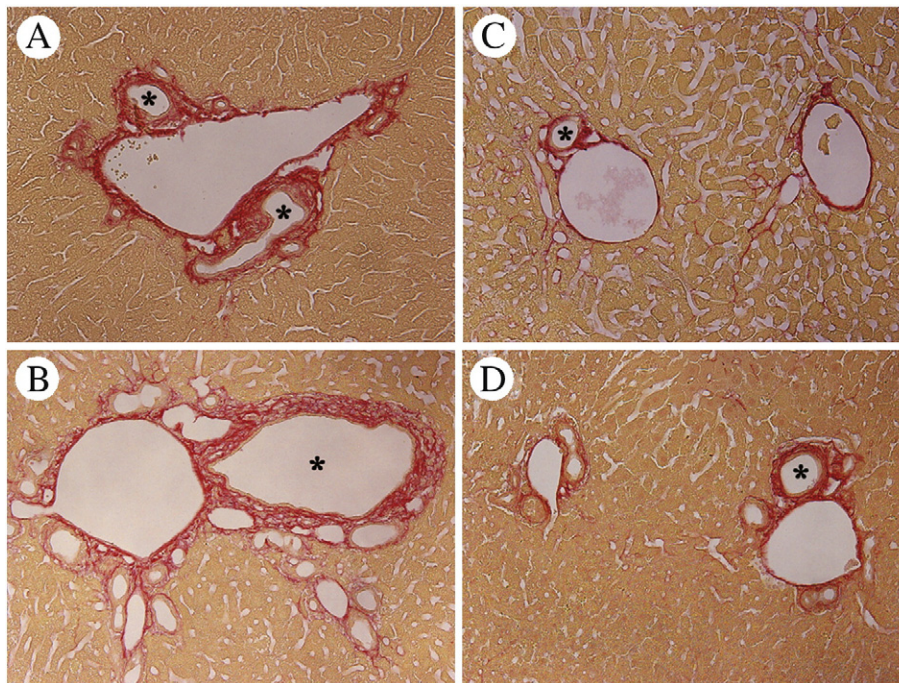

Fig. 1. Periductal fibrosis by common bile duct ligation. Collagen was stained using Sirius red (red stain) 7 (A and C) and 14 (B and D) days after common bile duct ligation. $Msn^{+/+}$ mice (A and B); $Msn^{-/-}$ mice (C and D). Bile duct proliferation and periductal collagen deposition were dominant in $Msn^{+/+}$ mice (A and B). In $Msn^{-/-}$ mice, collagen synthesis and proliferation were significantly reduced (C and D). Original magnification, ×200. Asterisk, bile duct.

HSCs were fixed in 100% methanol and permeabilized by 0.2% TritonX-100 avoiding autofluorescence for plenty of retinoids.

2.5. One-step real-time RT-PCR

Total RNA was extracted from whole liver with RNeasy kits (QIAGEN, Hilden, Germany). One-step real-time RT-PCR was per-

formed using Quantitect™ SYBR Green RT-PCR kit (QIAGEN) and Light Cycler 1.5 (Roche, Mannheim, Germany). Primers were designed by Primer Express Software (PE Applied Biosciences, CA, USA). For all primer pairs, specificity was confirmed by sequencing PCR products. Target gene levels are presented as a ratio of levels in BDL versus sham-operated groups (control), according to the ΔΔCt method. The primers used were as follows: GUS (NM_010368): forward,
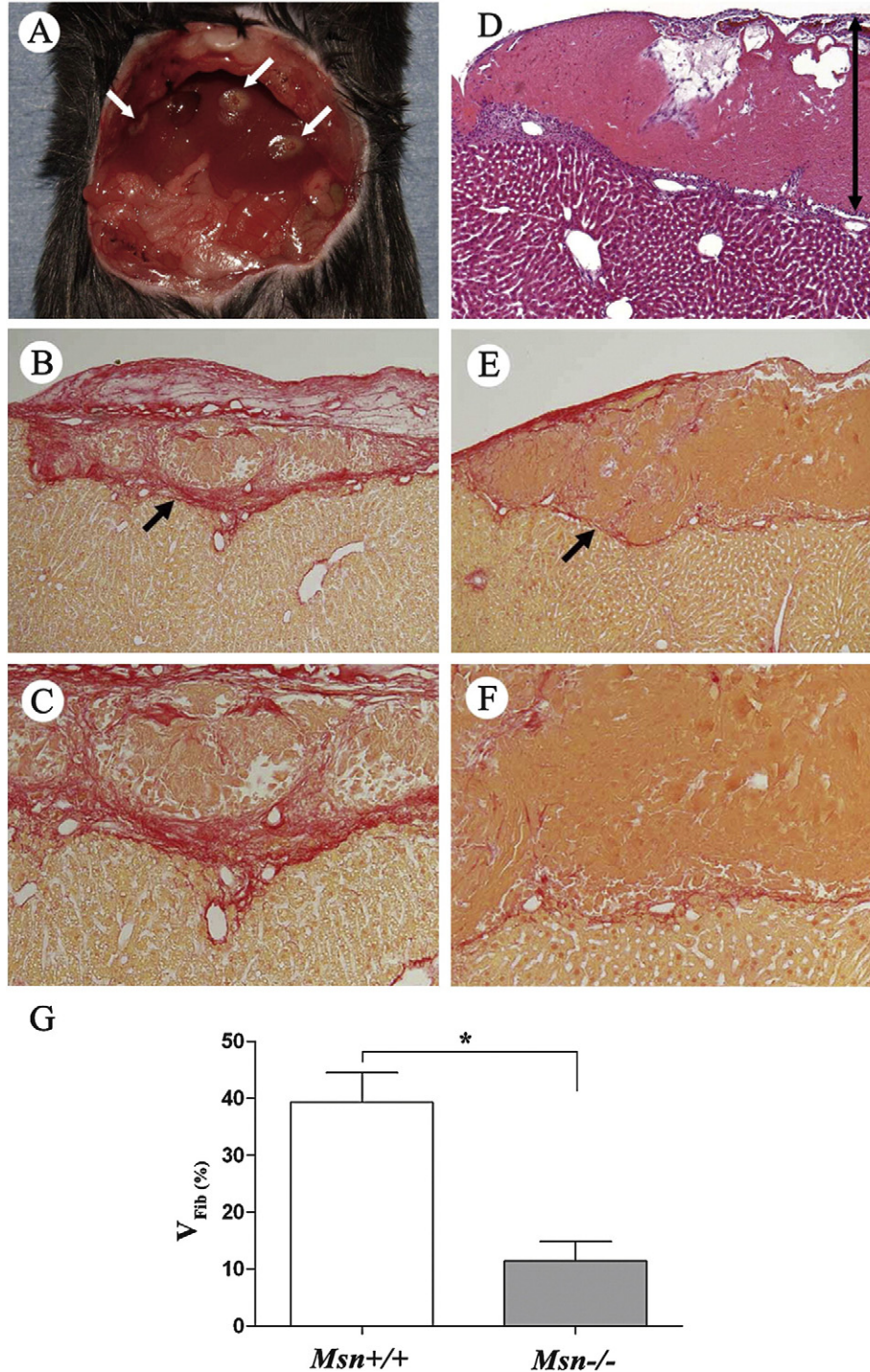
Fig. 2. Moesin deficiency reduced collagen synthesis in liver injury induced by heat cauterization. (A) Acute hepatic injury using a heated probe. Three individual lesions were created in each mouse liver (white arrow). The area of necrosis was ~3 mm. (D) The injury focus (black arrow) showed an inflammatory infiltrate and angiogenesis on day 7 after injury. HSCs are seen accumulating in $Msn^{+/+}$ mouse liver. Necrotic tissue was absorbed and replaced by fibrous tissue. Hematoxylin–eosin stain. Original magnification ×100. (B, C, E and F) Collagen was stained using Sirius Red (red stain) 14 days after focal thermal denaturation. $Msn^{+/+}$ mice (B and C); $Msn^{-/-}$ mice (E and F). Collagen fibers were abundant at the periphery of the injury (black arrow) in $Msn^{+/+}$ mice. In $Msn^{-/-}$ mice, collagen deposition was significantly reduced. Original magnification, ×100 (B and E), ×200 (C and F). (G) The amount of Sirius Red-positive tissues of focal thermal denaturation was determined as a percentage of section volume (V_{Fib}). The values were 39.3±5.2% ($Msn^{+/+}$) and 11.4±3.4% ($Msn^{-/-}$). *P<0.0001.

GCAGTTGTGTGGGTGAATGG; reverse, GGGTCAGTGTGTTGTTGATGG; αSMA (NM_007392): forward, AAACAGGAATACGACGAAG; reverse, CAGGAATGATTTGGAAAGGA: TGFb1 (NM_011577):NM_011577 forward, TTGCCCTCTACAACCAACACAA; reverse, GGCTTGCGACCCACG-TAGTA; procollagen Iα1NM_007742 (NM_007742): forward, GACATCCCTGAAGTCAGCTGC; reverse, TCCCTTGGGTCCCTCGAC; procollagen Iα2 (NM_007743): forward, CTCCAAGGAAATGGCAACTCAG; reverse, TCCTCATCCAGGTACGCAATG [9].

2.6. Immunoblotting

The liver was taken from $Msn^{+/+}$ and $Msn^{-/-}$ mice and homogenized in SDS sample buffer (50 mM Tris–HCl, pH 6.8, 2% SDS, 20% glycerol, 2% 2-mercaptoethanol and 0.01% bromophenol blue). Total lysate (20 μg) was separated by SDS-PAGE, and electrophoretically transferred from gels to PVDF membranes for immunoblotting. Immune complexes were detected using horseradish-conjugated goat anti-rabbit IgG fragments (dilution, 1:1000; DakoJapan, Tokyo, Japan) and the ECL Western blotting detection system (Amersham, Bucks, UK). We quantified the individual immunoblotted bands by comparing their intensities with those of serially-diluted reference standards for five separate combinations of $Msn^{+/+}$ and $Msn^{-/-}$ mice.

2.7. Image analysis

Image analysis for fibrosis was performed with Image J (National Institutes of Health, Bethesda, MD, USA) by three people blinded to the experimental protocol. The same background threshold was used in all specimens to distinguish black and white. Then, the amount of black and white was analyzed, and the percentage of white was recorded as the fibrosis volume (V_{Fib}), which was represented by Sirius red-positive tissue.

2.8. HSC isolation

In vivo-activated HSCs were isolated from common-bile-duct-ligated $Msn^{+/+}$ and $Msn^{-/-}$ mice 7days after operation. The liver was perfused with PBS that contained 100 IU/ml heparin (30 ml/h, 5min), 0.025% pronase (80 ml/h, 30 min), and 10.7 IU/ml collagenase (140ml/h, 30min). At the end of the perfusion period, the liver was removed and stirred with 0.001% DNase (37 °C, 30 min). HSCs were isolated on an 11.5% OptiPrep® density gradient. The purity of isolated HSCs was assessed as the percentage of cells that exhibited transient blue fluorescence under UV excitation. The average yield per liver was 1.0×10^6 cells with purity of 70–90%. The cells were plated in 20% FBS/DMEM.

2.9. HSC migration assay

Culture inserts were pre-coated with hyaluronic acid (1mg/ml), then rinsed with PBS before use. Isolated HSCs (1×10^3 cells/each cell culture insert) were plated in DMEM with 20% FBS. After 12 h, cell culture inserts were transferred to 24-well cluster plates in serum-free ASF 104 medium for the migration assay, as described previously. At the indicated times of migration, membranes were removed from the
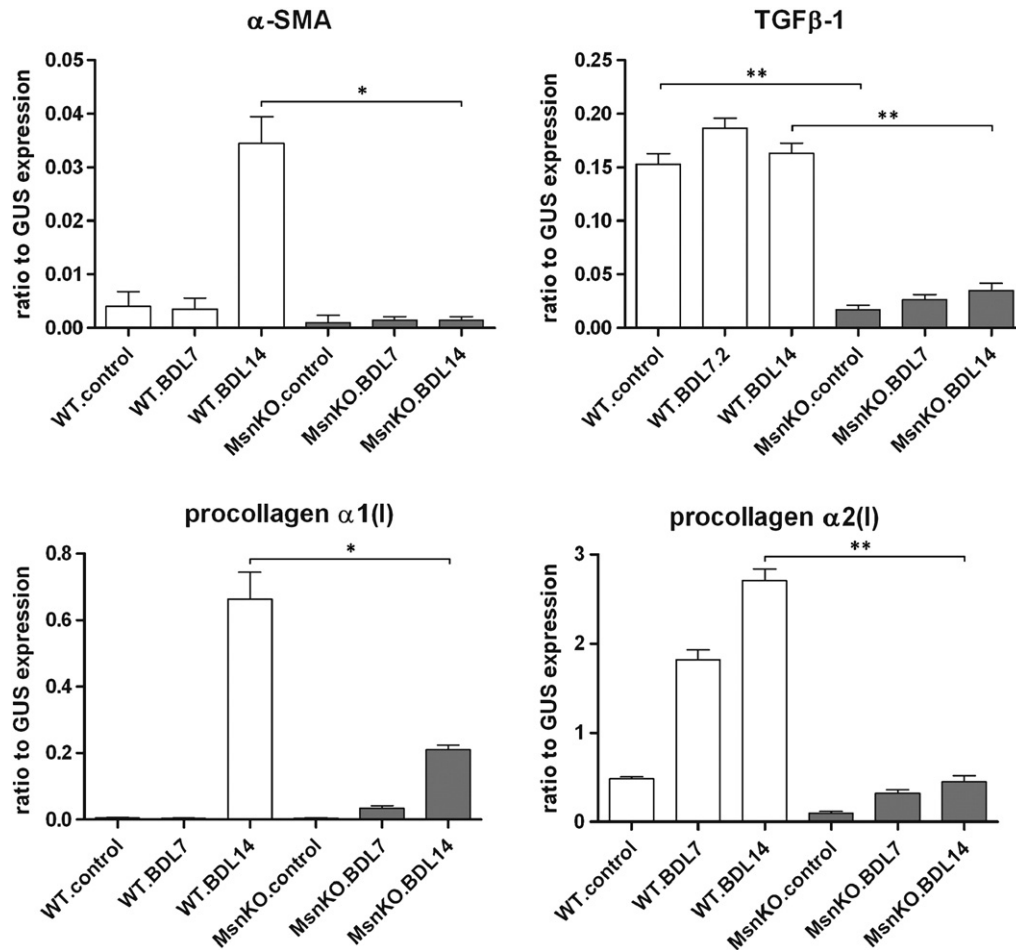
Fig. 3. Quantitative analysis of HSC activation and fibrosis in $Msn^{+/+}$ and $Msn^{-/-}$ mouse liver. mRNA levels of procollagen α2/α2(I), α-SMA and TGFβ-1 were determined by quantitative real-time PCR of total liver RNA obtained after 7 and 14 days of BDL or sham operation. Results were normalized to β-glucuronidase (GUS) expression in control (sham operation) mice. Expression of α-SMA, TGFβ-1 and procollagen α1/2(I) was significantly reduced in $Msn^{-/-}$ mouse liver at 7 and 14 days after BDL. *$P<0.05$, **$P<0.01$. Each experimental group consisted of control ($n=3$) and treated ($n=5$) mice. Data expressed as mean±SD data.

culture inserts, fixed in 4% phosphate-buffered formaldehyde and stained with hematoxylin. Migration was scored as the number of HSCs on the bottom of the membrane (Lw) and the top surface of membrane (Up), in the same fields at 400× magnification; each field contained about 10 cells, and 20 fields were assessed for each study. The migration index was (Lw/Up + Lw = %). Each experimental group consisted of five mice.

2.10. Statistical analysis

Results are expressed as means ± SD. Significance was established using Student's t test and analysis of variance. Differences were considered significant at $P < 0.05$. The data were analyzed by Graph Pad Prism5 (GraphPad Software, San Diego, CA, USA).

3. Results

3.1. Wound healing and liver fibrosis

Common bile duct ligation raises cholestasis and acute liver injury. In $Msn^{+/+}$ mouse liver collagen deposition and bile duct proliferation were significant around the intra-hepatic bile duct in zone 1 (red stain, Fig. 1A and B). Collagen synthesis and proliferation were reduced in $Msn^{-/-}$ mice (Fig. 1C and D). Focal thermal denaturation produced an injury with well-defined margins and a reproducible fibrotic response (Fig. 2A and D). In $Msn^{+/+}$ liver, the injury focus showed an inflammatory infiltrate and angiogenesis, followed by massive collagen production and fibrosis at the periphery (Fig. 2B and C). Generally, the injury resolved within 3 weeks. In $Msn^{-/-}$ mice, the inflammatory infiltrate and fibrosis at the injury margin within the liver were clearly reduced (Fig. 2E and F). Collagen deposition at the periphery of the lesion (Fig. 2B and E, black arrow) was quantified and found to be 39.3 ± 5.2% of the tissue section in $Msn^{+/+}$ but only 11.4 ± 3.4% in $Msn^{-/-}$ (Fig. 2G).

BDL and acute liver injuries increased markers of HSC activation, including expression of α2(I) and α2(I) procollagen, α-SMA and TGFβ-1 mRNAs (Fig. 3). HSC activation and procollagen synthesis were significantly reduced in $Msn^{-/-}$ mice.

3.2. ERM expression in mouse liver

In normal mouse livers, ezrin is expressed in cholangiocytes, radixin in bile canaliculi in hepatocytes, and moesin in endothelium or HSCs (Fig. 4A, D and G). BDL did not increase the expression of
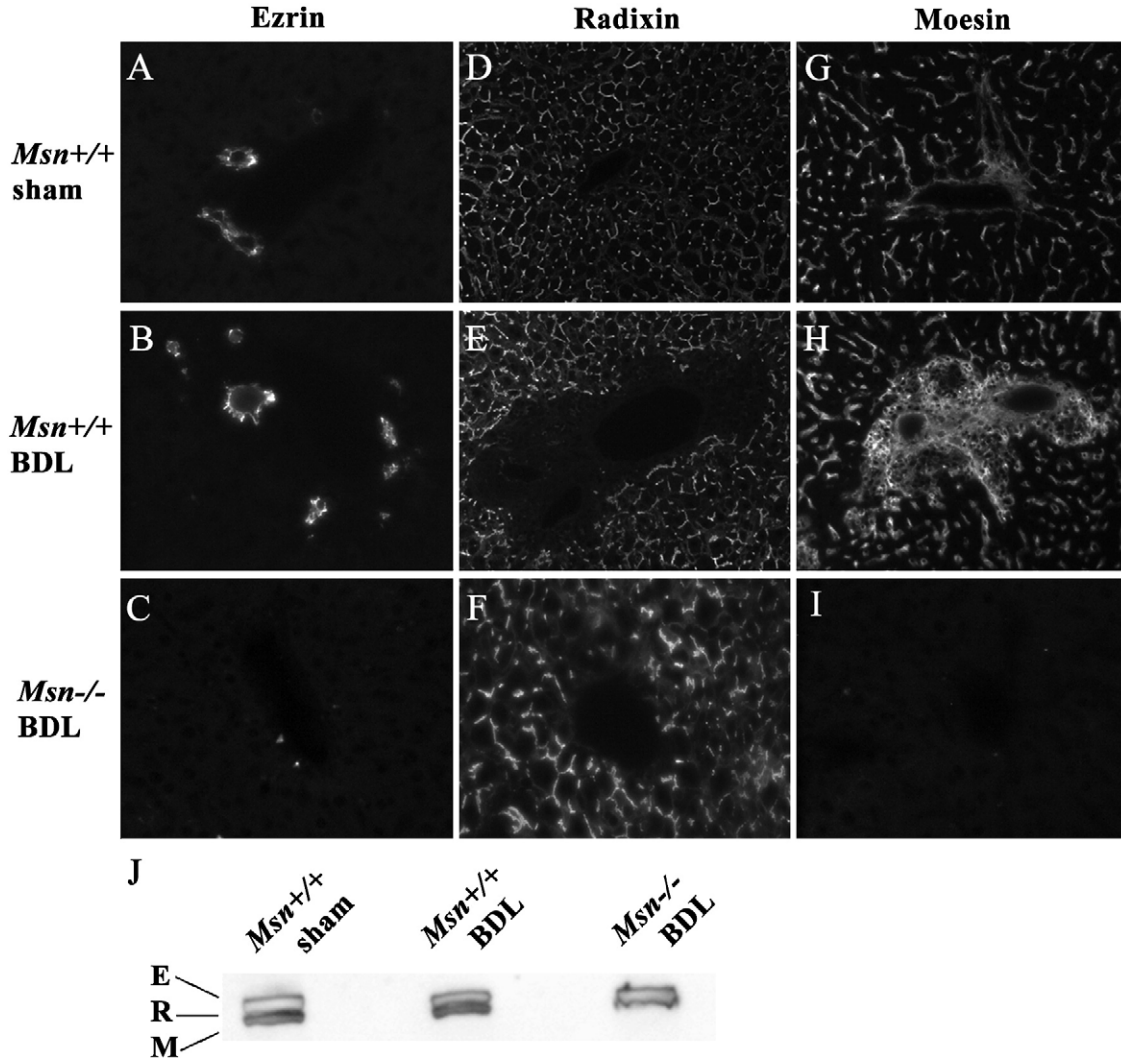
Fig. 4. ERM expression in mouse liver. (A–I) Immunofluorescent micrographs of frozen sections of the livers of $Msn^{+/+}$ (sham operation or BDL) and $Msn^{-/-}$ (BDL) mice 7 days after operation. ERM expression was unique in liver tissue: cholangiocytes, ezrin (A–C); bile canaliculi in hepatocytes, radixin (D–F); and endothelial cells, moesin (G and H). Moesin-positive cells increased in periductal areas in BDL $Msn^{+/+}$ mouse liver (H), but ezrin and radixin did not increase (B and E). Expression of ezrin and radixin was not compensatory in $Msn^{-/-}$ BDL mouse liver (C and F). Original magnification, ×200. (J) Immunoblotting. Acute liver injuries induced by BDL increased the amount of moesin in $Msn^{+/+}$ mice, but ezrin and radixin did not change in $Msn^{+/+}$ and $Msn^{-/-}$ mice. In each lane, 20 μg liver protein from $Msn^{+/+}$ and $Msn^{-/-}$ mice was loaded.
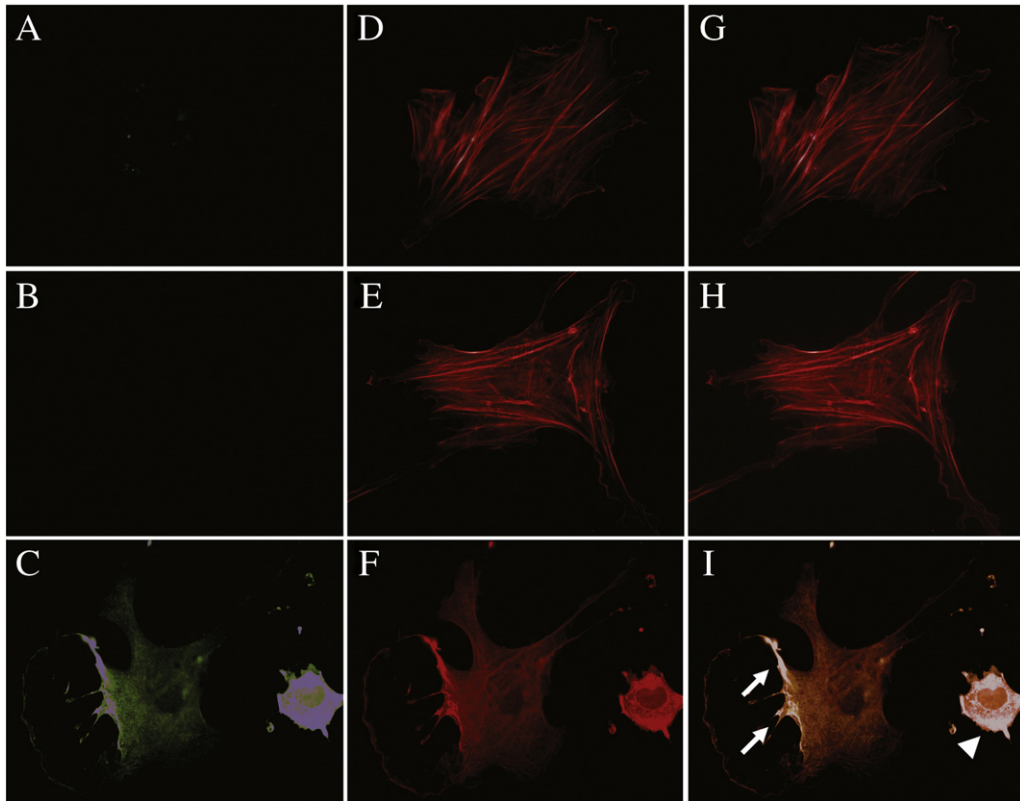
Fig. 5. ERM expression in HSCs. $Msn^{+/+}$ HSCs were isolated and placed in primary culture for 2 days. Ezrin (A), radixin (B) and moesin (C) are stained green. (D–F) Localization of α-SMA stained red. (G) Merged images of (A) and (D). (H) Merged images of (B) and (E). (I) Merged images of (C) and (F). In vivo-activated HSCs expressed moesin, but not ezrin or radixin (A–C). Moesin co-localized with α-SMA at the ruffling membrane of HSCs (C, F and I; white arrows). The expression level of moesin was greatest in compact HSCs, which are migration capable (I; white arrow head). Original magnification, ×400.

ezrin and radixin, but moesin-positive cells increased in zone 1 of $Msn^{+/+}$ mouse livers (Fig. 4B, E and H). Otherwise, ezrin and radixin did not compensate for moesin deficiencies in $Msn^{-/-}$ BDL liver (Fig. 4C, F and I). Expression of ERM proteins obtained by immunoblotting was almost consistent with the results of immuno-fluorescence microscopy. Moesin increased in $Msn^{+/+}$ BDL liver, but ezrin/radixin expression did not change in $Msn^{-/-}$ BDL livers (Fig. 4J).

3.3. ERM expression in HSCs

In vivo-activated HSCs expressed moesin but not ezrin or radixin (Fig. 5A–C). As expected of these linker proteins, moesin co-localized with α-SMA, notably at the ruffling membrane of HSCs (Fig. 5C, F and I; white arrows). Expression was particularly strong in tall and compact HSCs, which are the cells with the greatest mobility (Fig. 5I; white arrow head). The data suggest that linkage of moesin to α-SMA is essential for the reorganization of the cytoskeleton that occurs with activation of HSCs. We did not examine the ERM phenotype in culture-activated HSCs, because our previous study found that these cells lack migratory capability [2].

3.4. Migratory activity of HSCs

To confirm that activated HSCs from the $Msn^{-/-}$ liver were migration-impaired, we isolated cells from mouse liver that had been subjected to total ligation of the biliary duct, an injury that induces activation of HSCs within 4 days. The proportion of $Msn^{+/+}$ HSCs that migrated through the filter averaged 12.5 ± 0.1% at 24 h, and 22.1 ± 1.5% at 36 h. In sharp contrast, $Msn^{-/-}$ HSCs were almost completely quiescent, with a migration index of only 1.3 ± 1.2% at 36 h (Fig. 6). These data provide direct evidence for impaired migration of moesin-deficient HSCs.

4. Discussion

To the best of our knowledge, this is the first report of moesin being the ERM protein present in HSCs. Previous studies of this family of proteins in the liver have found that radixin is abundant in hepatocytes, ezrin in cholangiocytes and moesin in sinusoidal
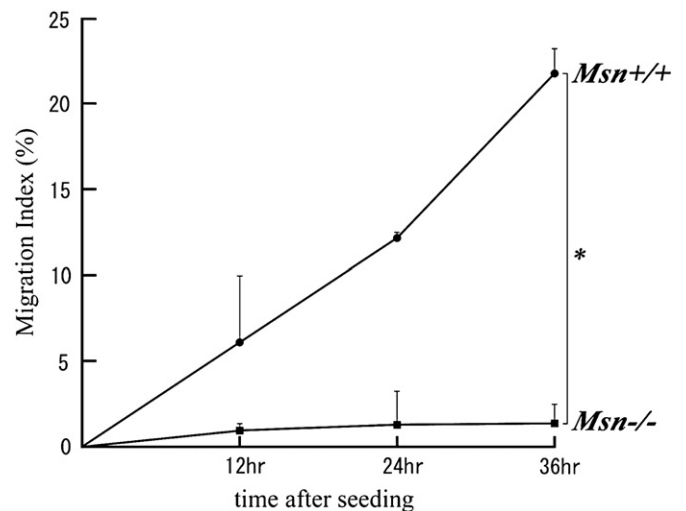
Fig. 6. Migration of HSCs depends on moesin. In vivo-activated HSCs were isolated from $Msn^{+/+}$ or $Msn^{-/-}$ mice after common bile duct ligation. HSCs were allowed to spread on hyaluronic-acid-coated cell culture inserts. The proportion of $Msn^{+/+}$ HSCs that migrated through the filter averaged 12.5±0.1% at 24 h, and 22.1±1.5% at 36 h. In contract, $Msn^{-/-}$ HSCs showed essentially no migration at 36 h. Migration index (%)=number of cells on the bottom surface/sum of cell numbers on upper and bottom surfaces. *$P<0.01$.

endothelial cells [10]. Interestingly, brain astrocytes, which share several properties with HSCs, express ezrin (and, in culture, radixin), but not moesin [11]. The counterpart of the HSC in the kidney is the mesangial cell, which reacts to injury by acquiring myofibroblast-like properties and producing collagens. It expresses both radixin and moesin [12]. The predominant linker protein in various types of fibroblasts in culture is ezrin [13]. We found that repair of the liver capsule (visceral peritoneum), in contrast to the parenchyma, was unaffected by moesin deficiency. Presumably, the capsule fibroblasts, which migrate from the abdominal cavity or ascites, utilize ezrin and/ or radixin. We examined the ERM phenotype of mouse embryo fibroblasts isolated from C57BL/6J mice (E15.5), and found that all three proteins were expressed (data not shown). Thus, it appears that expression of moesin alone may be unique to HSCs, just as individual ERM proteins are unique to other cell types in the liver (see above). The implications of exclusive expression of a single ERM family member by a specific cell type in the liver are speculative. The function of moesin in HSCs is likely to be similar to that of ERM proteins generally. These are linker proteins, which when phosphorylated are responsible for anchoring the actin cytoskeleton to the plasma membrane, and are particularly prominent in filopodia and microvilli of the plasma membrane [14]. An early facet of the injury response is migration of HSCs to the affected area. We have previously shown that HSCs use CD44 for migration on a substratum of hyaluronic acid [2]. ERM linker proteins are known to form a complex with CD44 and other migration-related proteins such as osteopontin [15]. They also likely participate in the formation of focal contacts between cell and substratum, which provide the traction for migratory movements. We now report that HSCs without moesin demonstrated minimal migratory capability.

Fibrogenesis by HSCs accompanies migration, although it is not clear whether these respective responses to injury are functionally linked. It is of interest in this regard that fibrogenesis was sharply attenuated in $Msn^{-/-}$ mice. In our study, moesin deficiencies reduced collagen deposition and bile duct proliferation in zone 1 and HSC activation. These findings indicated that moesin specifically interacts with membrane-associated proteins, some of which play important roles in HSC activation and fibrogenesis. It forms a complex with the beta receptor for platelet-derived growth factor (PDGF-Rβ). The ligand for this receptor, PDGF, is known to stimulate proliferation, migration and collagen production by HSCs [16–19]. Another member of the moesin–PDGF-R complex is sodium–hydrogen exchanger factor-1, which associates with G-protein-coupled receptors and receptor tyrosine kinase, which mediate intracellular signaling [20, 21]. Moesin appears to be required for the topographically and spatially correct formation of this complex. In its absence, the component proteins may drift within the plasma membrane and fail to generate the appropriate signals in response to the ligand, which leads to loss of the activation response. The expression of TGFβ-1 in Msn$^{-/-}$ control (sham operation) and $Msn^{-/-}$ BDL mice was significantly low. These results suggest that there is less fibrosis in $Msn^{-/-}$ mouse liver. The mechanism responsible for low levels of TGFβ-1 is still unclear. In the future, we would like to investigate actin dynamics and ERM function in HSCs when exposed to mitogens.

Progression in many chronic liver diseases can be characterized as inappropriately active or dysregulated repair, and the goal of many anti-fibrotic strategies is suppressing the repair response. The present results suggest that interventions that target moesin merit consideration. Despite their altered repair response, $Msn^{-/-}$ mice are phenotypically normal and fertile, which suggests that moesin is not critical for homeostasis in the adult [7]. In principle, this implies a margin of safety for agents that compromise moesin function in reactive HSCs, towards slowing disease progression in chronic liver injury.

References

[1] P. Tangkijvanich, S.P. Tam, H.F. Yee Jr., Wound-induced migration of rat hepatic stellate cells is modulated by endothelin-1 through rho-kinase-mediated alterations in the acto-myosin cytoskeleton, Hepatology 33 (2001) 74–80.

[2] S. Kikuchi, C.T. Griffin, S.S. Wang, D.M. Bissell, Role of CD44 in epithelial wound repair: migration of rat hepatic stellate cells utilizes hyaluronic acid and CD44v6, J. Biol. Chem. 280 (2005) 15398–15404.

[3] S. Charrin, A. Alcover, Role of ERM (ezrin–radixin–moesin) proteins in T lymphocyte polarization, immune synapse formation and in T cell receptor-mediated signaling, Front Biosci. 11 (2006) 1987–1997.

[4] F.C. Morales, Y. Takahashi, E.L. Kreimann, M.M. Georgescu, Ezrin–radixin–moesin (ERM)-binding phosphoprotein 50 organizes ERM proteins at the apical membrane of polarized epithelia, Proc. Natl. Acad. Sci. U. S. A. 101 (2004) 17705–17710.

[5] F.C. Morales, Y. Takahashi, S. Momin, H. Adams, X. Chen, M.M. Georgescu, NHERF1/EBP50 head-to-tail intramolecular interaction masks association with PDZ domain ligands, Mol. Cell. Biol. 27 (2007) 2527–2537.

[6] S. Yonemura, M. Hirao, Y. Doi, N. Takahashi, T. Kondo, S. Tsukita, S. Tsukita, Ezrin/radixin/moesin (ERM) proteins bind to a positively charged amino acid cluster in the juxta-membrane cytoplasmic domain of CD44, CD43, and ICAM-2, J. Cell. Biol. 140 (1998) 885–895.

[7] Y. Doi, M. Itoh, S. Yonemura, S. Ishihara, H. Takano, T. Noda, S. Tsukita, Normal development of mice and unimpaired cell adhesion/cell motility/actin-based cytoskeleton without compensatory up-regulation of ezrin or radixin in moesin gene knockout, J. Biol. Chem. 274 (1999) 2315–2321.

[8] S. Kitajiri, K. Fukumoto, M. Hata, H. Sasaki, T. Katsuno, T. Nakagawa, J. Ito, S. Tsukita, S. Tsukita, Radixin deficiency causes deafness associated with progressive degeneration of cochlear stereocilia, J. Cell. Biol. 166 (2004) 559–570.

[9] K. Yamaguchi, L. Yang, S. McCall, J. Huang, X.X. Yu, S.K. Pandey, S. Bhanot, B.P. Monia, Y.X. Li, A.M. Diehl, Diacylglycerol acyltranferase 1 anti-sense oligonucleotides reduce hepatic fibrosis in mice with nonalcoholic steatohepatitis, Hepatology 47 (2008) 625–635.

[10] L. Fouassier, C.Y. Duan, A.P. Feranchak, C.H. Yun, E. Sutherland, F. Simon, J.G. Fitz, R.B. Doctor, Ezrin–radixin–moesin-binding phosphoprotein 50 is expressed at the apical membrane of rat liver epithelia, Hepatology 33 (2001) 166–176.

[11] A. Derouiche, M. Frotscher, Peripheral astrocyte processes: monitoring by selective immunostaining for the actin-binding ERM proteins, Glia 36 (2001) 330–341.

[12] C. Hugo, C. Hugo, R. Pichler, K. Gordon, R. Schmidt, M. Amieva, W.G. Couser, H. Furthmayr, R.J. Johnson, The cytoskeletal linking proteins, moesin and radixin, are upregulated by platelet-derived growth factor, but not basic fibroblast growth factor in experimental mesangial proliferative glomerulonephritis, J. Clin. Invest. 97 (1996) 2499–2508.

[13] R.F. Lamb, B.W. Ozanne, C. Roy, L. McGarry, C. Stipp, P. Mangeat, D.G. Jay, Essential functions of ezrin in maintenance of cell shape and lamellipodial extension in normal and transformed fibroblasts, Curr. Biol. 7 (1997) 682–688.

[14] S. Tsukita, K. Oishi, N. Sato, J. Sagara, A. Kawai, S. Tsukita, ERM family members as molecular linkers between the cell surface glycoprotein CD44 and actin-based cytoskeletons, J. Cell. Biol. 126 (1994) 391–401.

[15] R. Zohar, N. Suzuki, K. Suzuki, P. Arora, M. Glogauer, C.A. McCulloch, J. Sodek, Intracellular osteopontin is an integral component of the CD44–ERM complex involved in cell migration, J. Cell. Physiol. 184 (2000) 118–130.

[16] E. Borkham-Kamphorst, J. Herrmann, D. Stoll, J. Treptau, A.M. Gressner, R. Weiskirchen, Dominant-negative soluble PDGF-beta receptor inhibits hepatic stellate cell activation and attenuates liver fibrosis, Lab. Invest. 84 (2004) 766–777.

[17] E. Borkham-Kamphorst, C.R. van Roeyen, T. Ostendorf, J. Floege, A.M. Gressner, R. Weiskirchen, Pro-fibrogenic potential of PDGF-D in liver fibrosis, J. Hepatol. 46 (2007) 1064–1074.

[18] S.L. Friedman, M.J. Arthur, Activation of cultured rat hepatic lipocytes by Kupffer cell conditioned medium. Direct enhancement of matrix synthesis and stimulation of cell, J. Clin. Invest. 84 (6) (1989) 1780–1785.

[19] N. Kinnman, R. Hultcrantz, V. Barbu, C. Rey, D. Wendum, R. Poupon, C. Housset, PDGF-mediated chemoattraction of hepatic stellate cells by bile duct segments in cholestatic liver injury, Lab. Invest. 80 (2000) 697–707.

[20] M.F. James, R.L. Beauchamp, N. Manchanda, A. Kazlauskas, V. Ramesh, A NHERF binding site links the betaPDGFR to the cytoskeleton and regulates cell spreading and migration, J. Cell. Sci. 117 (2004) 2951–2961.

[21] K.L. Wu, S. Khan, S. Lakhe-Reddy, G. Jarad, A. Mukherjee, C.A. Obejero-Paz, M. Konieczkowski, J.R. Sedor, J.R. Schelling, The NHE1 Na+/H+ exchanger recruits ezrin/radixin/moesin proteins to regulate Akt-dependent cell survival, J. Biol. Chem. 279 (2004) 26280–26286.